SCHLIEREN IMAGING BASED 2-D TEMPERATURE FIELD RECONSTRUCTION OF LAMINAR NATURAL CONVECTIVE AIR FROM VERTICAL HEATED PLATE

Rohit Gupta[1,*] , Chayan Das[1], Ranjan Ganguly[1], Amitava Datta[1]

[1] Department of Power Engineering, Jadavpur University, Kolkata-700098, India
*Corresponding author – rohit.ju.pe@gmail.com

Abstract. Light rays undergo refraction when it passes through a region of optical inhomogenity i.e. through a density gradient. This forms the basis of Schlieren imaging. Different methods have been used to visualize and quantify different flow fields of interest over several decades. Recent developments in computational image processing algorithms have made an evolution to this imaging technique. In this paper we attempt to visualize the natural convective boundary layer of a heated vertical plate and reconstruct two dimensional (2-D) temperature data by two different methods experimentally: one is Toepler's lens based Schlieren (LBS) with knife edge cutoff and the other one is Background oriented Schlieren (BOS) imaging. In order validate the accuracy of reconstructed temperature field, similar environment was simulated by computational fluid dynamics (CFD) simulation in ANSYS FLUENT and also by thermocouple traverse method experimentally. The presented temperature field shows the accuracy of the adopted methodology.

Keywords: Background oriented Schlieren (BOS) imaging, Knife-edge cutoff, Temperature field reconstruction, Natural Convection.

1 Introduction:-

Non-intrusive optical measurements based on Schlieren imaging technique offer avenues of indirect measurement complex temperature gradient field of air flows since it leads to local gradient in the refractive index of the air [1]. The Schlieren effect was suggested in 1930s by Schmidt [2] and Schardin [3] which can be used to measure refraction and thus calculating the change in concentration or temperature of the flow field.

Quantitative Schlieren imaging was proposed much before the computer era but its application was limited due to requirement of densitometry and integration by hand. Researcher's preferred inteferometry at that time. Modern computers can now acquire, process and post-process all the Schlieren images.

A wide range of publications in the Schlieren imaging literature reports a number of techniques applied to various flow fields. The most popular method in the pre-

computer era, lens-based Schlieren image with knife-edge cut-off, now utilizes computational image processing to produce accurate result [4]. Although the lens-based methods were extensively studied in past few decades, it had certain drawbacks. Data extractions from large flow-fields were limited by the diameter of the lens (large diameter, aberration-free lenses are prohibitively expensive). Further developments by Meier [5] and Dalziel [6] introduced a new technique called synthetic Schlieren which overcame the drawbacks of large scale flow visualization. This technique has gained popularity in the name of background oriented Schlieren (BOS).

There are very few such publications in the literature that explicitly compare the relative drawbacks of one method over the other [7,8]. Elsinga et al. [7] compared BOS and color Schlieren results for investigating the density field in a supersonic wind tunnel. Both produced results within about 2% of the known theoretical curves. Hargather et al. [8] compared BOS, knife-edge Schlieren and color Schlieren for studying a natural convective air plume form a heated vertical plate. The BOS technique suffered problem of limited resolution because the background and the test section were not sharply focused simultaneously. Therefore, we believe that a better image acquisition and processing techniques are to be developed.

Several other researchers have attempted the study of natural convective air plume from horizontal plate using knife edge calibration curve [9,10], convective air field within a vertical channel [11] and convective water flow within the same [12].

The authors hereby compare two quantitative Schlieren imaging techniques: lens-based Schlieren (LBS) with knife-edge cutoff and BOS in order to study the simple refractive two-dimensional steady flow fields of a free convection laminar boundary layer on a heated vertical plate, as was done in [8]. This classical heat transfer problem avoids issues regarding vibrations of the glass windows and wind tunnel that confine the flow. The study is further bolstered by presenting a comparison between the theoretical profile [13] obtained through CFD simulations using ANSYS FLUENT 17.2 and also through intrusive measurement of the temperature profile by thermocouple. This article also proposes the modified algorithms and possible development in order to synthesize more accurate BOS images.

2. Theoretical background:-

2.1 Laminar free-convection boundary layer of vertical plate:-

The laminar free convection vertical plate boundary layer problem was solved theoretically by Ostrach [13] using a similarity solution to relate the non-dimensional temperatures and velocity parameters to length parameter η. The similarity parameter η combines the distance y from the plate leading edge, and the perpendicular distance x from the plate surface, and also the Grashoff number at a particular distance from the leading edge, such that

$$\eta = \left(\frac{Gr_y}{4} \right)^{1/4} \frac{x}{y} \tag{1}$$

The nondimensional temperature distribution in the thermal boundary layer is given by the function θ as

$$\theta(\eta) = \frac{T - T_a}{T_w - T_a} \quad \textbf{(2)}$$

The tabulated theoretical data by Ostrach at $Pr = 0.72$ is used for validating the CFD results at different local Rayleigh numbers (Ra_y), where

$$Ra_y = Gr_y . \Pr , \quad \textbf{(3)}$$

and $Gr_y = \frac{g\beta(T_w - T_a)y^3}{\nu^2}, \Pr = \frac{\nu}{\alpha}$.

Here g denotes the gravitational acceleration, T_w is the plate surface temperature, T_a is the free stream air-temperature, ν, is the free-stream air kinematic viscosity, α is the thermal diffusivity and β is the coefficient of thermal expansion, evaluated as $\beta = \frac{2}{T_w + T_a}$.

2.2 Mathematical and optical modeling of Toepler's lens based Schlieren (LBS) imaging system:-

Light rays passing through a transparent medium of varying refractive-index gradients [4]. Fig 1 shows a schematic top view where light is shown to be refracted in x-direction due to the hot thermal boundary layer in the vicinity of a vertical plate of length Z. A light ray traveling in the z-direction is refracted through an angle ϕ_x due to the refractive-index gradient in the x-direction. For a two dimensional phase object of extent Z this is quantified as:

$$\varepsilon_x = \frac{1}{n}\int_0^Z \frac{\partial n}{\partial x} dz = \frac{Z}{n_\infty}\frac{\partial n}{\partial x} \quad \textbf{(4)}$$

The refractive index and temperature can be related by coupling the Gladstone-dale equation and the equation of state:

$$n = 1 + \frac{GP}{RT} \quad \textbf{(5)}$$

Where, n = refractive index, G = Gladstone-Dale constant dependent on wavelength of light, P = atmospheric pressure $= 1.01325 \times 10^5$ N/m^2, R = ideal gas constant for air = 0.287 kJ/kgK, T = absolute temperature of air (K). The value of $G(\lambda)$ is calculated from [4] the equation:

$$G(\lambda) = 2.2244 \times 10^{-4}\left[1 + \left(\frac{6.7132 \times 10^{-8}}{\lambda}\right)^2\right] \quad \textbf{(6)}$$

where the wavelength of white light source is taken a, $\lambda = 589$ nm.

The density-gradient field within a gas can thus be directly quantified by measuring the refractive-index gradient field, which is obtained through each of the two experimental techniques presented here.

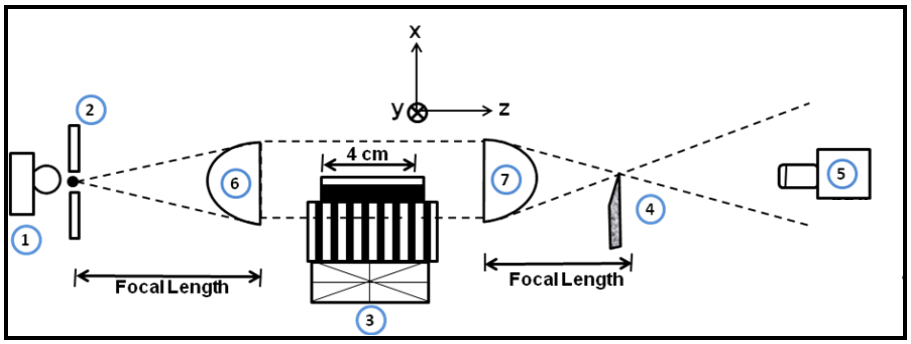

Fig. 1: Schematic of the Toepler's lens based Schlieren imaging setup. **Legends: (1)** White light source, **(2)** Irish Diaphragm, (**3**) Test Specimenn (Heated plate), **(4)** Knife-edge, **(5)** DSLR Camera with lens, (**6**) Collimating Plano Convex Lens, **(7)** Decollimating Plano Convex Lens.

The classical double pass lens-based Schlieren system (see Fig. 1) employs a non-coherent tungsten halogen white light source of 250 Watt and wavelength, λ = 589 nm from a point source which is eventually controlled by regulating an aperture and passing the light through a fiber optic source. A first plano-convex lens with 75 mm diameter and a focal length of f_c = 500 mm collimates the light to a beam diameter of 45 mm, which passes through the region having a refractive index gradient. The collimated light then passes through a second plano-convex lens with 75 mm diameter and focal length f_d = 500 mm, and gets de-collimated. The magnification at the image output plane is thus $M = (f_d/f_c) = 1$. A knife-edge mounted on a three axis traverse is placed at the focal point of the de-collimating plano-convex lens. This is termed as the output plane of the Schlieren image. The knife edge acts as a Hilbert transform [4] and blocks selective frequencies of the Fourier spatial frequency spectrum based on its shape. This forms the Schlieren images at the output plane. A Nikon digital SLR 7200 mounted with *f* 18-140 mm telephoto lens acquires the images. The camera is sharply focused at the location of test object. A broad range of cameras could also have been used, but a camera with high pixel resolution and a large pixel-bit depth is desired to maximize spatial resolution and ability to resolve a greater range of pixel intensities [8]. For ensuring proper alignment all the optical accessories are mounted on an optical rail situated on an optical breadboard.

2.3 Mathematical and optical modeling background oriented Schlieren (BOS) imaging system:-

An image "*I*" of an object is a convolution of the background or object function "*B*" and the transfer channel function "*T*" [5]:

$$I = B * T \tag{7}$$

The de-convolution will describe the transfer channel if the object and the image are given. The most convenient situation is given in the case of a comparison of a background with no distortion with one which has the distorted transfer channel. This procedure provides reasonably detailed information on the deflector in the transfer channel, depending upon the accuracy in the process of de-convolution and imaging. By the process of de-convolution a two-dimensional integral deflection map of the phase object is achieved, which is very similar to a bidirectional Schlieren picture or a Synthetic Schlieren (SS) image. The refractive index field is governed by the same

beam deflection equation (Eq. 4). The only difference in between BOS and LBS is that in LBS the beam deflection angle is quantified by studying the DPIS and in BOS it is by measuring the amount of virtual pixel shift.
In reality, BOS setup is a much more simplified setup than Toepler's method. It utilises a diverging white light source illuminating an artificially generated randomly spaced black speckles of a certain diameter printed on a white background and a digital SLR camera mounted with a lens. In presence of a phase object the black dots suffer virtual shift in the direction of refractive index gradient which is extract by computerised image processing algorithms. It is worth mentioning that the amount of deflection at the output plane is largely dependent on the distances from the screen to the camera and the screen to phase object. Despite of having several advantages over classical LBS system, BOS suffers several problems such as diverging light source, focusing on the screen and the phase object at the same time. The authors have found solution to the problem of focusing on both the objects at the same time. It is seen that keeping the shutter speed and ISO sensitivity constant if the *f*-number i.e the aperture stop of the lens is increased then the depth of field is increased. As a result, the phase object and the screen both stay sharply at the focus. It is worth mentioning that all the BOS images are captured at the maximum value of aperture stop i.e., *f*36 available for the Nikon 7200 DSLR camera used in the experiment.

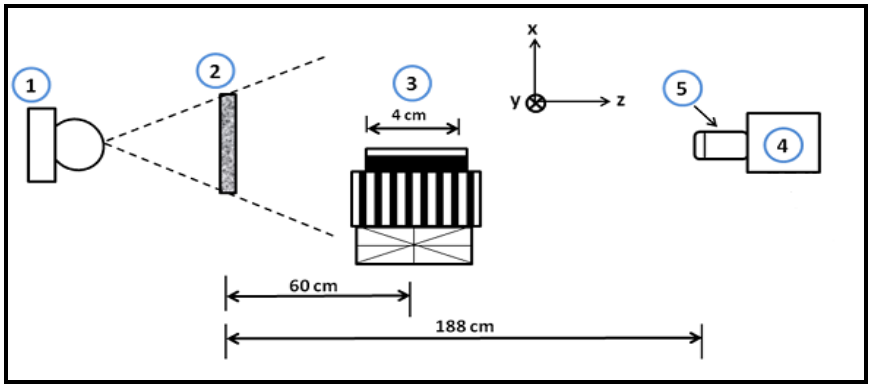

Fig. 2: Schematic of the BOS setup**. Legends: (1)** White light source, **(2)** Background pattern (randomly spaced black dots on white paper), **(3)** Test Specimen (Heated vertical plate), **(4)** Camera, **(5)** Lens.

2.4 CFD simulation of steady laminar natural convection boundary layer of heated vertical plate:-

Schlieren data are validated through a CFD code using commercial software (ANSYS Fluent 17.2). Simulations were performed in a 2-D free convection configuration to capture the boundary layer profile next to a heated vertical plate. A 2-D (quadrilateral grid), steady flow was solved using laminar model. Phase coupled SIMPLE scheme is used for pressure-velocity coupling and second order upwind scheme is chosen to discretize the governing equations.

The computational domain and grid structure is shown in Fig. 3, Temperature profiles are reported along the imaginary line A-A'.

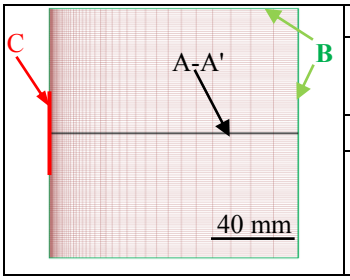

Boundary condition	
• **B** - Pressure inlet: 1 bar, Specified T) • **C** - Test plate (wall): Specified T, No-slip	
Properties of air	
Density (kg/m^3)	Ideal-gas
Specific heat	1006.43(J/kg.K)
Thermal conductivity	0.0242 (W/m.K)
Viscosity	1.789×10^{-5}(Kg/m.sec)

Fig. 3: Computational domain and the boundary conditions. Field variables are reported along the imaginary line A-A'.

3. Experimental setup and data extraction methodology:-

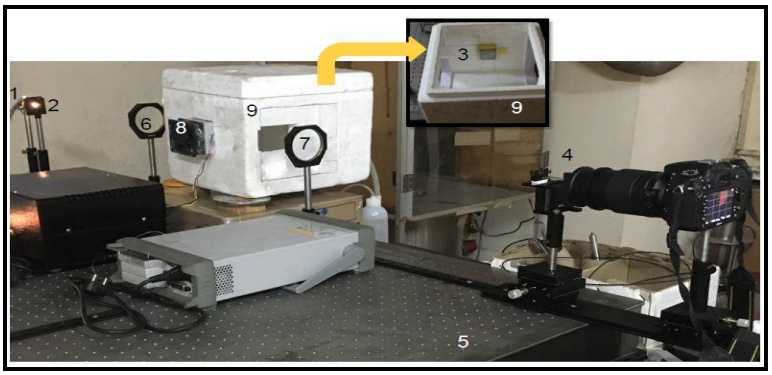

Fig. 4: Experimental setup**. Legends: (1)** White light source, **(2)** Irish Diaphragm, **(3)** Test Specimen, **(4)** Knife-edge, **(5)** Optical breadboard, **(6)** Collimating plano-convex Lens, **(7)** De-collimating plano-convex Lens, **(8)** Heat-sink with cooling fan arrangement, **(9)** Styrofoam box for flow isolation.

The specimen that is studied here with the help of two Schlieren imaging techniques is a natural convective air rising from a heated vertical plate. A Peltier-heat sink arrangement equipped with a cooling fan is mounted on a Styrofoam chamber (see Fig. 4). The Peltier arrangement is mounted in a groove within the styrofoam wall which in turn heats up a copper block of dimension $40\times40\times50$ mm^3. An aluminum plate (the test plate) of dimension $40\times40\times5$ mm^3 is mounted vertically with a help of thermal paste (Make – Omegatherm) in order to ensure sufficient thermal contact at the copper block-aluminum plate interface. The Peltier element is driven by a variable DC power supply and the cooling fan rotates at a constant rpm in order to extract a certain amount of heat from the heat sink. The plate is driven at two different voltages in order to maintain two different plate surface temperatures and thus at two different Rayleigh numbers. A K type the thermocouple (Make – Omega) is mounted at the copper block – vertical plate interface in order to measure the plate temperature. Another K-type thermocouple is mounted at a distance of 120 mm from the plate surface for measuring the free-stream air temperature. All the experiments are

performed after the plate has reached a steady state temperature and the temperature fluctuation read by the thermocouple is within ± 0.1°C. A third K-type thermocouple, mounted on a 3-axis traverse, is traversed in discrete steps along the vertical plate surface, thus measuring the plate temperature physically. The light ray pass along *z*-axis, *x* is the outward distance from plate and *y* is along the distance from the leading edge of the plate. The acquired images are processed by an in-house image processing code written in MATLAB. The algorithms developed for two different Schlieren imaging methods are described next.

3.1 Algorithm for extracting 2-D temperature field by LBS imaging:-

Step I - Two images are captured, one in presence of phase disturbance (flow effect) and another in absence of phase disturbance (background image).
Step II – Both the images are converted to grayscale format from RGB format in order to obtain the pixel intensity values across the pixels.
Step III – After conversion, the grayscale image intensity matrix with phase object is subtracted from the image intensity matrix without phase object. As a result of the operation the differential pixel intensity spectrum (DPIS) is obtained, which clearly displays the boundary layer of a vertical plate.
Step IV – Further examination of DPIS indicates that the pixels near the plate have higher values which gradually decrease away from the plate. This forms the basis of the contrast spectrum which is shown later (Fig. 7) in form of a contour plot
Step V - During the experiments, the average plate temperature and average ambient temperature were obtained from thermocouple readings which were used to scale the DPIS matrix within the temperature limits.

3.2 Algorithm for extracting 2-D temperature field by BOS imaging:-

Step I –Two BOS images were captured, one in presence of phase disturbance (flow effect) and another in absence of phase disturbance.
Step II – Cross correlation method which is generally popular in PIV based flow analysis was used to extract the apparent shift of pixel, which is caused by the refractive index gradient in *x* and *y* directions. As a result of cross-correlation, one obtains two discrete matrices which contain pixel shifts along *x* and *y* directions, respectively. This was plotted as a vector field, and is termed as pixel displacement field. The matrix which contains the information about pixel shifts in *x*-direction can clearly quantify about the boundary layer thickness and temperature profile.
Step III – By knowing the refractive index adjacent to the plate surface from plate temperature and ambient refractive index from ambient temperature, the Poisson equation of refractive index (Eq. 8) within the image domain was solved in order to obtain full field of refractive index.

$$\frac{\partial^2 n}{\partial x^2} = \frac{\partial(\Delta x)}{\partial x} \tag{8}$$

Where, Δx = the amount of pixel shift obtained from cross-correlation which contains gradient of refractive index perpendicular to the plate.
Step IV – After obtaining the full field of refractive index form the displacement field, the density field was reconstructed from the refractive index data, which in turn was used to obtain full field temperature.

4. Results and discussion:-

4.1 Benchmarking the CFD results with Ostrach's theoretical solution:

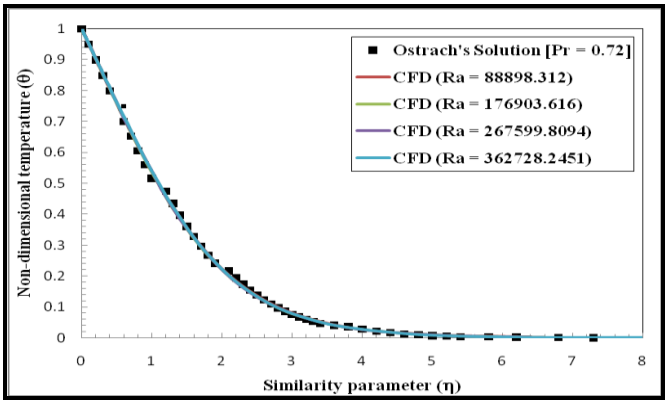

Fig. 5: Non-dimensional temperature distribution (θ) plotted as a function of the Ostrach [13] similarity parameter (η) that combines local Grashoff number (Gr_y), perpendicular distance from plate (x) and distance from the leading edge (y).

The CFD data was used to validate the temperature reconstruction from Schlieren imaging are benchmarked against the Ostrach's theoretical solution at Pr = 0.72. CFD simulations were performed at four different Rayleigh numbers and non-dimensional temperature distribution (θ) was plotted as a function of the similarity parameter (η). Fig. 5 shows an excellent agreement in between CFD simulation and Ostrach's theoretical solution.

4.2 Comparison of thermocouple traverse data and CFD results:

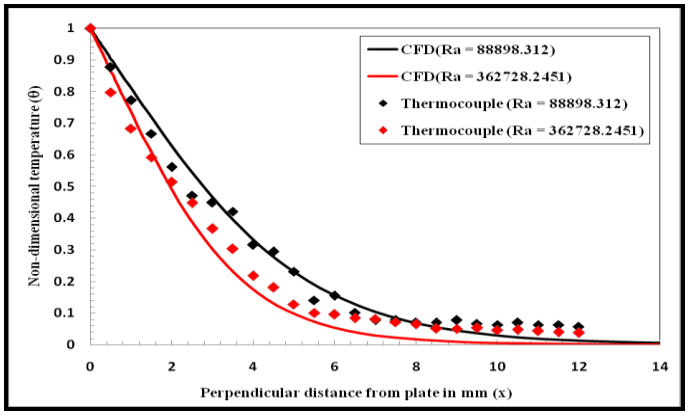

Fig. 6: Comparison of CFD results with thermocouple traverse data (at the mid-point of plate)

Non-dimensional temperature distribution obtained from CFD results are further compared experimentally by traversing a thermocouple mounted on a three axis traverse at different surface temperatures. Figure 6 shows a comparison of the validation results at the highest and lowest local Rayleigh numbers (Ra_y). It can be

clearly concluded form the temperature distribution that when the Rayleigh number is higher the temperature distribution away from the vertical surface drops sharply because of an increment in buoyancy driven convective force.

4.3 Comparison of Schlieren and CFD results.

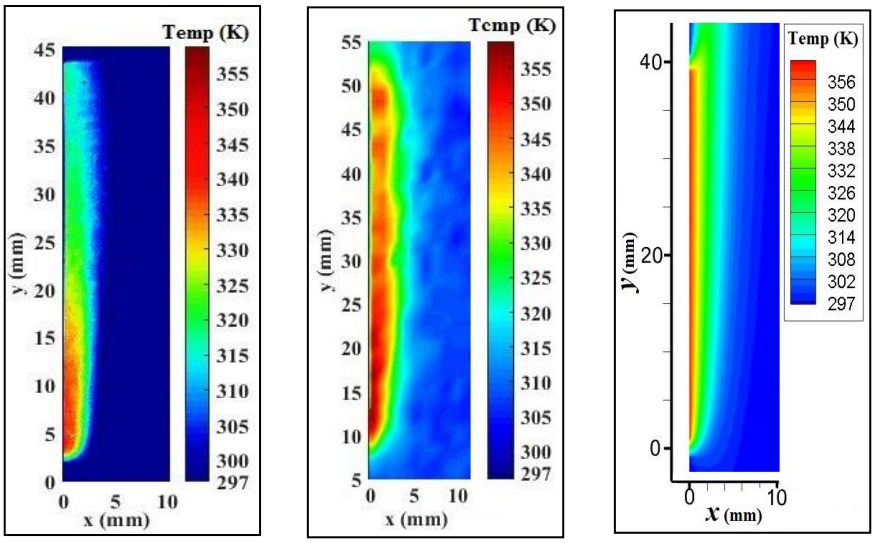

Fig. 7: Reconstructed 2-D temperature contours from LBS (left), BOS (mid) and CFD (right) results

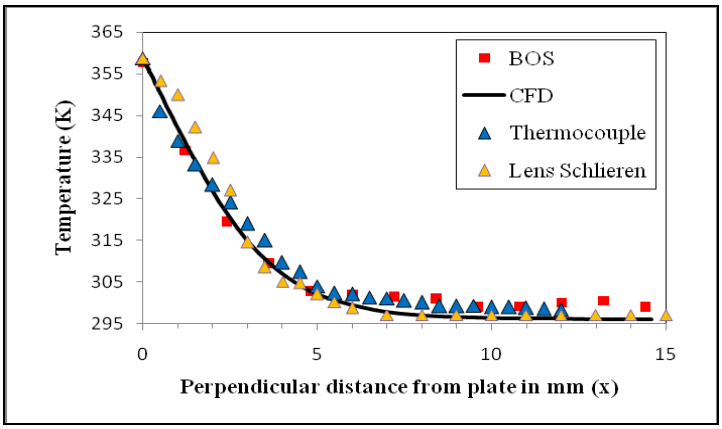

Fig. 8: Comparison of temperature distribution plotted as a function of perpendicular distance from plate obtained from LBS imaging, BOS imaging, CFD simulation and thermocouple readings (at *Ra* = 362728.2451)

The thermal boundary layer in perpendicular direction to the plate can be clearly visualized from the temperature reconstruction data (see Fig. 7). Quantitative results are also obtained regarding spatial variation of temperature. All the reconstruction data shown in Fig. 7 and Fig. 8 corresponds to T_w = 358.8 K and T_a = 297 K. It can be

inferred from the temperature contours that, while capturing the steep gradient of temperature in the boundary layer, the BOS method slightly overpredicts the ambient temperature. This happens because the local scalar gradients of refractive index field are too weak to produce meaningful data by PIV cross-correlation. However the LBS method captures the ambient condition correctly.

5. Conclusion:-

Both the Schlieren techniques extensively studied here produced meaningful temperature reconstruction data which were validated against physical temperature measurement, CFD simulation and a classical theoretical solution, thereby verifying the accuracy of the proposed algorithms. Possible improvements to some of the optical aspects were also suggested that would result in acquisition of better Schlieren images at the solid boundary-gas interaction surface.

References

1. Panigrahi P.K, Muralidhar K. Schlieren and Shadowgraph Methods in Heat and Mass Transfer, Springer Briefs in Thermal Engineering and Appied Science, DOI: 10.1007/978-1-4614-4535-7_2.
2. Schmidt E. Schlierenaufnahmen des temperaturfeldes in der nahe wormeab - gebender korper. Forschung auf dem Gebiete des Ingenieurwesens 1932;3(4):181–9.
3. Schardin H. Das toeplersche Schlierenverfahren: Grundlagen fur seine anwendung und quantitative auswertung. VDI-Forschungsheft No. 367 1934;5(4):1–32.
4. Settles G.S. Schlieren and shadowgraph techniques: visualizing phenomena in transparent media. Springer-Verlag; 2001.
5. Meier G.E.A. Computerized background-oriented Schlieren. Experiments in Fluids (2002) 33. 181–187.
6. Dalziel SB, Hughes GO, Sutherland BR. Synthetic Schlieren. In: Carlomagno GM, editor, Proc. 8th international symposium on flow visualization, vol. 62, Sorrento, Italy; 1998.
7. Elsinga GE, Oudheusden BWV, Scarano F, Watt DW. Assessment and application of quantitative Schlieren methods: calibrated color Schlieren and background oriented Schlieren. Experiments in Fluids 2004;36(2):309–25.
8. Hargather M.J, Settles G.S. A comparison of three quantitative Schlieren techniques. Optics and Lasers in Engineering 50 (2012) 8–17
9. Martínez-González A., Moreno-Hernández D., and Guerrero-Viramontes J. A.. Measurement of temperature and velocity fields in a convective fluid flow in air using Schlieren images. APPLIED OPTICS (2013) Vol. 52, No. 22. 5562-5569.
10. C. Alvarez-Herrera, D.Moreno-Herna´ndez , B.Barrientos-Garcia, J.A.Guerrero-Viramontes Temperature measurement of air convection using a Schlieren system. Optics & Laser Technology 41 (2009) 233–240.
11. Tanda G, Devia F. Application of a Schlieren technique to heat transfer measurements in free-convection. Experiments in Fluids 24 (1998) 285–290.
12. Tanda G, Fossa M, Misale M. Heat transfer measurements in water using a Schlieren technique. International Journal of Heat and Mass Transfer 71 (2014) 451–458.
13. Ostrach S. An analysis of laminar free-convection flow and heat transfer about a flat plate parallel to the direction of the generating body force. Technical Report 2635, NACA; 1952.